

A human parietal face area contains aligned head-centered visual and tactile maps

Martin I Sereno¹ & Ruey-Song Huang^{1,2}

Visually guided eating, biting and kissing, and avoiding objects moving toward the face and toward which the face moves require prompt, coordinated processing of spatial visual and somatosensory information in order to protect the face and the brain. Single-cell recordings in parietal cortex have identified multisensory neurons with spatially restricted, aligned visual and somatosensory receptive fields, but so far, there has been no evidence for a topographic map in this area. Here we mapped the organization of a multisensory parietal face area in humans by acquiring functional magnetic resonance images while varying the polar angle of facial air puffs and close-up visual stimuli. We found aligned maps of tactile and near-face visual stimuli at the highest level of human association cortex—namely, in the superior part of the postcentral sulcus. We show that this area may code the location of visual stimuli with respect to the face, not with respect to the retina.

In macaque monkeys, neurons in a multisensory parietal area at the border between visual cortex and somatosensory cortex—the ventral intraparietal area, VIP—have spatially restricted visual and somatosensory receptive fields that are aligned with each other¹. For example, a VIP neuron with a visual receptive field in the upper right part of the visual field will also typically have a somatosensory receptive field located on the upper right part of the forehead. VIP neurons respond selectively to optical flow stimuli^{2,3} and have connections with visual motion areas, somatosensory areas and motor areas controlling face and eye movements^{4,5}. Electrical stimulation of VIP results in defensive movements including flinching⁶.

The mobility of the eyes with respect to the face and head, however, could potentially misalign somatosensory and visual inputs^{7,8}. There is evidence that some VIP neurons remap their visual receptive fields to cancel the effects of eye movements^{1,9}, by using information about eye position. Thus, if the monkey moves its eyes downward so that the visual stimulus moves farther into the upper visual field with respect to the eye, the visual receptive field will nevertheless maintain its alignment with the upper right forehead rather than moving downward with the eye. These VIP neurons thus represent both visual and somatosensory information in a somatosensory coordinate system. This is in contrast to the nearby lateral intraparietal area (LIP), which represents and updates potential visual targets—including those initially detected by way of another modality—in a visual (retinotopic) coordinate system^{10,11}.

Previous functional magnetic resonance imaging (fMRI) studies of multisensory processing in humans^{12,13} have shown using conjunction analysis that there is a small region in parietal cortex that responds to somatosensory, visual and auditory stimuli just as monkey VIP does. In both humans and monkeys, however, there has been no evidence that

this region contains retinotopic or somatotopic maps of near-face space. Earlier studies of LIP in humans, which is situated just posterior to the multisensory focus, showed that there, potential visual targets are in fact represented in a retinotopic cortical map^{14–16}. This study set out to determine if human VIP, too, contains a topographic map—but in this case, a multisensory map in which visual space is superimposed and aligned with a somatosensory map.

RESULTS

Subjects ($n = 12$) were posed in the scanner with their heads tilted slightly forward so that they could directly view (without a mirror) a wide-field visual stimulus projected onto a translucent back-projection screen located very close to the face. The tilt also made it possible to deliver gentle, computer-controlled air puffs to 12 approximately equally spaced locations around the face, through adjustable plastic nozzles (see Fig. 1; the near-face back-projection screen has been removed in Fig. 1g). Subjects wore ear plugs, and white noise was delivered via magnetic resonance (MR)-compatible headphones in order to completely mask the sound of the air puffs. Data were analyzed using surface-based Fourier methods¹⁷.

Identification of a new parietal face area

First, we used four different block-design stimulus protocols (Fig. 1a–d) to identify multisensory areas of interest (Fig. 2a) and to make a connection with previous studies. The first of these, ‘Whole face air puffs versus OFF’ (Fig. 2b, data shown on dorsolateral view of inflated surface), compared 16-s periods in which air puffs were delivered to random locations on the face to 16-s periods of nothing. The experiment was conducted in the dark and subjects kept their eyes closed. As expected, this strongly activated face primary somatosensory

¹Department of Cognitive Science, and ²Swartz Center for Computational Neuroscience, Institute for Neural Computation, University of California San Diego, La Jolla, California 92093, USA. Correspondence should be addressed to M.I.S. (sereno@cogsci.ucsd.edu).

Received 11 August; accepted 1 September; published online 24 September 2006; doi:10.1038/nn1777

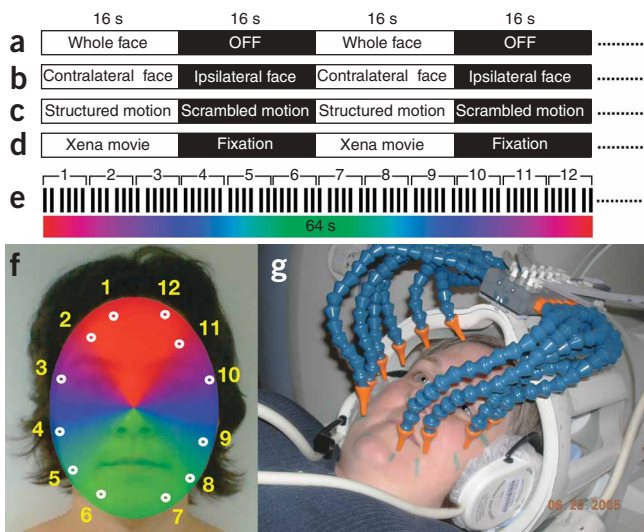


Figure 1 Experimental protocols and stimulus apparatus. (a–e) Four two-condition block-design protocols (a–d) and a phase-encoded air-puff protocol (e) (top). (f,g) In the protocols shown in a, b and e, trains of gentle air puffs with occasional longer gaps were delivered by adjustable air tubes to 12 different locations (f) on each person's face (g). Visual stimuli were presented on a close-up, direct-view back projection screen (not shown). The color coding scheme used for the somatosensory maps in **Figures 3–6** are shown in e and f (numbers in e correspond to locations in f). Black bars in e represent 100-ms air puffs (not drawn to scale) with 100-ms or 200-ms interstimulus gaps.

cortex (areas 3b and 1) on the posterior bank of the central sulcus as well as secondary somatosensory cortex (areas S-II and PV, not visible in this view) on the upper bank of the lateral sulcus. Another area in superior parietal cortex (dotted red circles in **Fig. 2b**) was bilaterally activated as strongly (3–5% peak-to-peak signal amplitude) as primary somatosensory cortex. This area was located at the confluence of the postcentral and intraparietal sulci, near “region 1” in ref. 12. Very similar results were obtained when subjects maintained central fixation on an otherwise blank screen instead of keeping their eyes closed (data not shown).

In a second block-design experiment, we compared air puffs delivered to random locations on the right versus the left half of the face (again in the dark). We found similarly strong activations in primary and secondary somatosensory cortex, but also in the superior parietal focus. A number of regions were significantly more strongly activated by stimulation of the contralateral face than the ipsilateral face (**Fig. 2c**), and no region was more strongly activated by stimulation of the ipsilateral face. This result is expected in primary and secondary somatosensory areas, as these areas are known to have receptive fields mainly on the contralateral half of the skin surface, but this was also the case in the superior parietal region, indicating that this area might be somatotopic as well.

The third and fourth block-design experiments showed that the superior parietal region is also strongly visually responsive (in the figure, circles are in same position across all conditions to aid comparisons). While fixating a central cross, subjects viewed structured moving random dot fields (dilations, contractions, spirals and rotations) versus scrambled moving dot controls. Both resulted in strong

activation in parts of areas V3A and V6 (ref. 18) and the anterior parts of the MT complex (possibly similar to macaque area MSTd). The optical flow stimulus also activated several parietal regions, including both LIP+ (refs. 14,19) and the region previously activated by the air puffs (**Fig. 2d**). The latter was also strongly activated when subjects viewed a naturalistic moving visual scene (portions of episodes of a television action show) while fixating a central cross (relative to periods in which subjects fixated the central cross against a black background). This last protocol was used to outline the entire extent of visually driven cortex (ref. 20 and **Fig. 2e**).

Aligned multisensory maps

To determine whether the multisensory superior parietal focus contained aligned somatosensory and visual maps, we did two additional experiments. First, we adapted a stimulus method initially developed for mapping retinotopic visual polar angle representations^{17,21} to the somatosensory system. A computer-controlled train of air puffs successively visited each of 12 locations around the face (multiple short

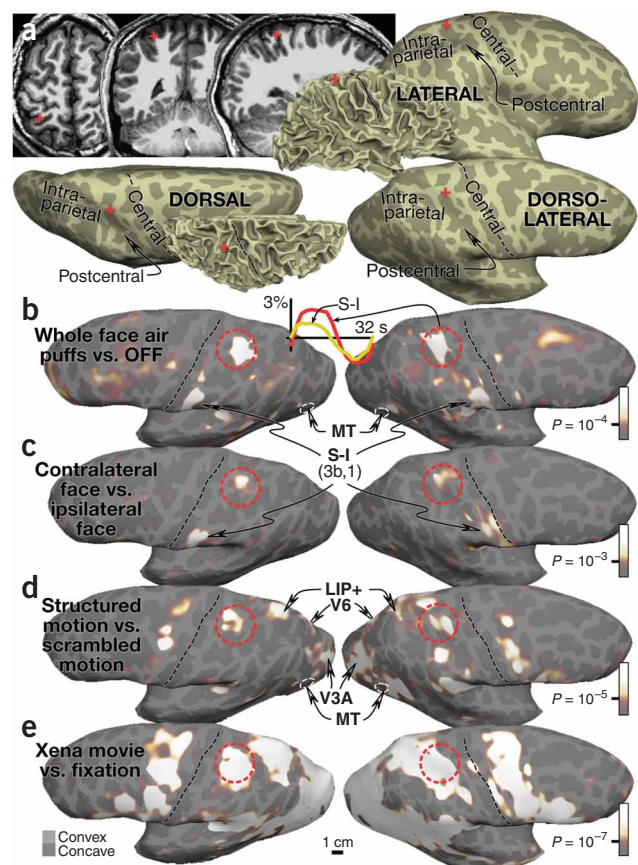


Figure 2 Somatosensory and visual stimuli activate a multisensory area in superior parietal cortex. (a) The location of the multisensory focus (red crosses) is indicated in slice view and on folded and unfolded cortical surface reconstructions of the right hemisphere. (b–e) Results of somatosensory (b,c) and visual (d,e) block-design experiments are shown for both hemispheres of a single person. The superior parietal multisensory region is indicated by the red dashed circles, which are in equivalent positions to aid comparison. The single-voxel time courses in b show that air puffs activated the circled area as strongly as they did primary somatosensory cortex (S-I). The multisensory region was located in the superior part of the postcentral sulcus and on its anterior bank. Whereas visual stimulation activated virtually the entire occipital lobe (e), occipital activation by somatosensory stimuli was confined to a region at the anterior end of the MT complex (b), possibly corresponding to area MSTd.

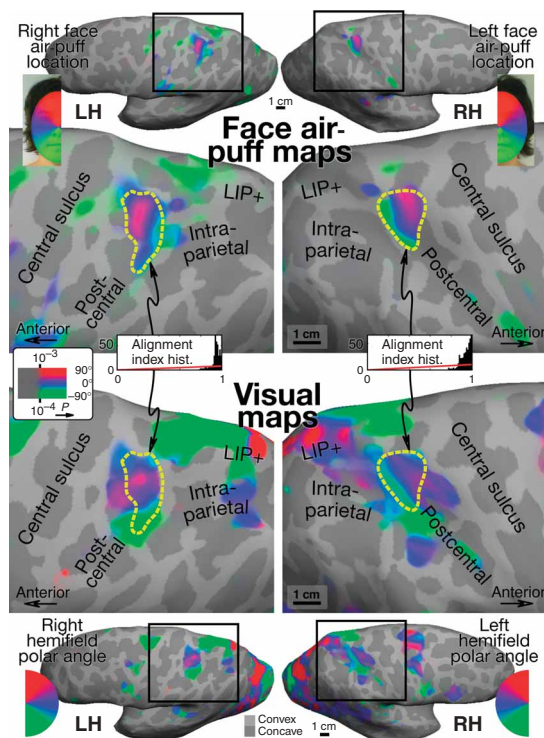


Figure 3 Aligned somatosensory and visual maps for a single subject (dorsolateral view). Top, results of somatosensory mapping by air puffs. Bottom, results of visual mapping by close-up rotating wedges containing video stimuli. Black rectangles (top, bottom) indicate the position of the higher magnification views in the center of the figure. Thick dashed yellow contours outline a region of interest defined as a connected surface patch of superior parietal vertices with significant periodic response to both somatosensory and visual mapping stimuli. In this region, the upper part of the contralateral face (top rows, red) is overlaid by a representation of the upper contralateral visual field (bottom rows, red). A similar alignment is visible for middle (blue) and lower (green) face and visual field. The alignment index histogram (see Methods) shows the distribution of agreement in polar angle for each vertex within the yellow contour (an index of 1 indicates no difference in phase angle between two maps). The red line indicates the estimated alignment index distribution (given the number of vertices and histogram bins) if the two maps within the yellow contour were completely uncorrelated.

In both hemispheres (**Fig. 3**, top), an area in the superior parietal cortex showed a strong somatotopic response to the air-puff mapping protocol (**Fig. 1e,f**). The map was located at the confluence of the postcentral and intraparietal sulci. In this region, the upper parts of the face are represented anterior to the lower parts of the face on the unfolded cortex (**Supplementary Video 1** online). Note that Fourier-based methods only show areas with differential responses to facial stimulus location; regions that respond to every air puff are ‘subtracted out’.

We also collected data from a visual mapping experiment in a separate scanning session with the same subject (**Fig. 3**). The close-up video mapping stimuli activated a number of retinotopic visual areas in posterior parietal, occipital and posterior inferotemporal lobes (last two not visible in this view), all of which had been silent during the somatosensory stimuli. The video stimuli also activated several areas in superior parietal cortex, one of which overlapped the map uncovered by the air-puff stimuli. Notably, the representation of visual stimulus angle closely matched the representation of facial air-puff stimulus angle. Upper visual fields were found anterior to lower

puffs at each location, **Fig. 1f**), starting near the midline of the forehead and slowly cycling once around the face every 64 s (there were eight such cycles per scan). Subjects monitored for occasional temporal irregularities in the sequence. To improve the signal-to-noise ratio, we averaged four such scans for each subject. To correct for systematic regional variations in the shape of the hemodynamic response function, we interleaved clockwise and counterclockwise progressions (two scans each) and then combined opposite-direction data by vector addition of the complex-valued signal (the strength and phase of the response at the stimulus frequency) after reversing the phase of one direction. The somatosensory maps were then compared with maps generated during retinotopic mapping experiments in the same subjects in a different session. For these experiments, we used video stimuli that were displayed within rotating wedges (as before, four-scan averages, two clockwise, and two counterclockwise). By projecting the visual stimuli onto the close-up direct-view screen, we were able to survey a much larger field of view (100° visual angle) than is typical for retinotopic mapping experiments. This was critical in order to map the part of the visual field that would typically be stimulated by a naturalistic visual object that got close enough to the face to touch the parts of the face that our air puffs did.

We conducted a combined somatosensory and visual mapping experiment on the unfolded cortical surface of one person (**Fig. 3**). Somatosensory stimuli were delivered in the dark with the eyes closed.

Figure 4 Visual somatosensory alignment for four additional subjects. The results of somatosensory mapping by air puffs (top) and visual mapping by close-up rotating wedges containing video stimuli (bottom) are shown for single hemispheres of four additional persons, in dorsolateral view. The dashed yellow contours represent the multisensory region of interest and are in equivalent positions for each hemisphere to aid comparison. Similar to the results in **Figure 3**, there was a detailed within-subject correspondence between somatosensory and visual maps (see alignment histograms). Other conventions follow **Figure 3**.

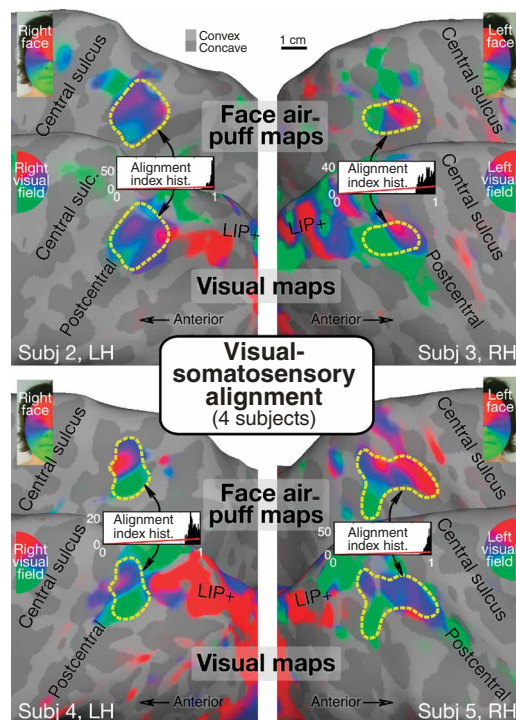


Table 1 Polar angle correlations (vertex by vertex), standard deviations of angular offsets, and average alignment indices across each region of interest shown in Figures 3–6 (see Methods)

| Subj, Hemi | Number of vertices | Corr* | Std. dev. | Avg. align. ind. |
|--|--------------------|-------|----------------|------------------|
| Map alignment: retinotopic/air-puff-o-topic | | | | |
| Subj 1, LH | 372 | 0.71 | $\pm 12^\circ$ | 0.95 |
| Subj 1, RH | 451 | 0.58 | $\pm 13^\circ$ | 0.94 |
| Subj 2, LH | 426 | 0.76 | $\pm 7^\circ$ | 0.97 |
| Subj 3, RH | 490 | 0.71 | $\pm 18^\circ$ | 0.91 |
| Subj 4, LH | 269 | 0.97 | $\pm 15^\circ$ | 0.93 |
| Subj 5, RH | 465 | 0.95 | $\pm 7^\circ$ | 0.97 |
| Subj 6, LH | 372 | 0.75 | $\pm 14^\circ$ | 0.94 |
| Subj 7, RH | 382 | 0.54 | $\pm 11^\circ$ | 0.95 |
| Avg (9), LH | 601 | 0.27 | $\pm 11^\circ$ | 0.95 |
| Avg (9), RH | 660 | 0.89 | $\pm 6^\circ$ | 0.97 |
| Map alignment: retinotopic/gaze-o-topic | | | | |
| Subj 6, LH | 372 | 0.70 | $\pm 9^\circ$ | 0.93 |
| Subj 7, RH | 382 | 0.36 | $\pm 12^\circ$ | 0.94 |
| Map alignment: air-puff-o-topic/gaze-o-topic | | | | |
| Subj 6, LH | 372 | 0.50 | $\pm 18^\circ$ | 0.93 |
| Subj 7, RH | 382 | 0.65 | $\pm 10^\circ$ | 0.96 |

* $P < 10^{-10}$.

visual fields, suggesting that in this region, somatosensory and visual maps are superimposed and aligned with respect to polar angle.

To quantitatively compare the alignment of the somatosensory and visual maps, we calculated an alignment index that ranged from 0 (π offset) to 1 (perfectly aligned) for each vertex in the multisensory region of interest (dashed yellow lines) for the two data sets (Methods). In both hemispheres, the distribution of alignment indices had a sharp peak near 1 (aligned), and the somatosensory and visual polar angle maps were strongly and significantly correlated (Table 1, Subj 1).

The quantitative agreement between the maps is within the limit of resolution of our mapping method, which is constrained by functional scan voxel width (~ 3 mm), cross-session alignment accuracy (~ 1.5 mm), and visual/somatosensory stimulus alignment accuracy ($\sim 15^\circ$ polar angle). The portion of the retinal sensory surface activated by visual stimuli was somewhat larger than the portion of facial sensory surface activated by the air puffs. The slowly rotating wedge used for visual mapping extended from near the center of the face as well as the scalp, ears, neck, shoulders and arms, which are known to activate some monkey VIP neurons. This may explain why the visual maps extend slightly anterior to the somato-

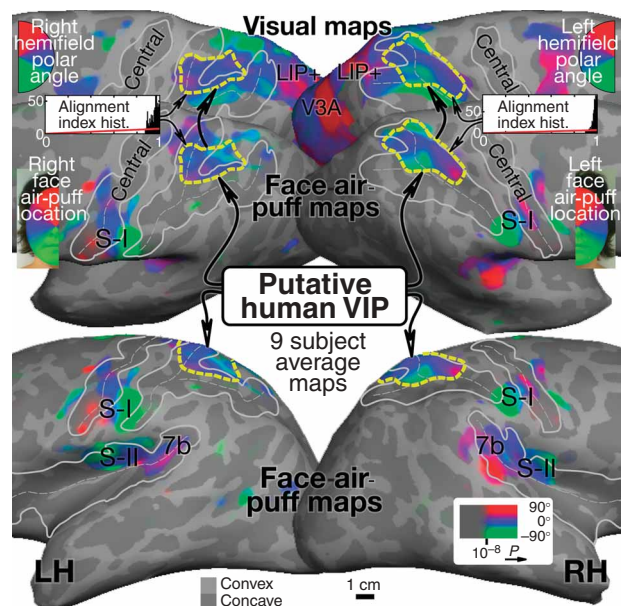
Figure 5 Surface-based average visual and somatotopic maps from nine subjects. The thick dashed yellow outline marks the new superior parietal multisensory map of polar angle of face stimulation and visual stimulation in putative human VIP. The complex-valued mapping data were averaged in a spherical surface coordinate system after morphing each subject's data into alignment with an average spherical sulcal pattern, and were then displayed back on the unfolded cortical surface of one person (Subj 1, illustrated in Figs. 2 and 3). The visual data is shown in dorsolateral view (top) and the somatosensory data is shown in dorsolateral (middle) and lateral (bottom) views. The maps of these two modalities were well aligned (alignment histograms at top); upper parts of the contralateral face and visual field (red) were situated anterior to middle (blue) and lower (green) parts of the face and visual field. The boundaries of the central sulcus and the confluence of the postcentral and intraparietal sulci are outlined in gray; sulcal fundi are dashed.

sensory maps. The additional space between LIP+ and VIP in humans as compared to monkeys is not unprecedented—for example, in humans, strongly motion-sensitive V3A is separated from V2 by another area, whereas in monkeys, direction-selective V3 (or DM) touches V2 directly.

Somatosensory and visual mapping data from four additional subjects (Fig. 4) showed that the location and organization of the area putatively identified as human VIP was similar across subjects, though the exact details of the maps varied between subjects. For example, the upper face (and upper visual field) were situated anterior to the lower face (and lower visual) field in subjects 3, 4 and 5, but subject 2 (upper left) had a doubled representation. However, when comparing somatosensory and visual maps within subjects, the agreement was quite remarkable; for example, the somatosensory and visual maps were doubled in precisely identical ways in subject 2. The visual impression of map similarity was confirmed by the quantitative alignment index distributions, which were all sharply peaked near 1 (see also Table 1).

Average visual and face air-puff maps

To average mapping data across subjects, we first inflated each person's cortical surface to a sphere and then morphed it into alignment with an average spherical cortical surface using FreeSurfer²². This automatic, iterative, nonlinear method quantitatively aligns major sulci while also minimizing metric (local angle and local areal) distortion across the surface. Complex-valued mapping signals were then combined across subjects on a vertex-by-vertex basis by vector averaging²³, and displayed on the unfolded hemispheres of one subject. We obtained the average somatosensory and visual mapping data from nine subjects (Fig. 5). Alignment histograms and correlations (Table 1) showed that the average visual and face air-puff maps were very well aligned, with anteriorly placed representations of the upper visual field and forehead. The data suggest that putative human VIP might contain more than one representation of the face (and visual field), especially in the right hemisphere. In this respect, VIP may be similar to LIP+, which has recently been found to have multiple subdivisions in both monkeys²⁴ and humans¹⁹. Higher resolution scans will be required to settle this question definitively.



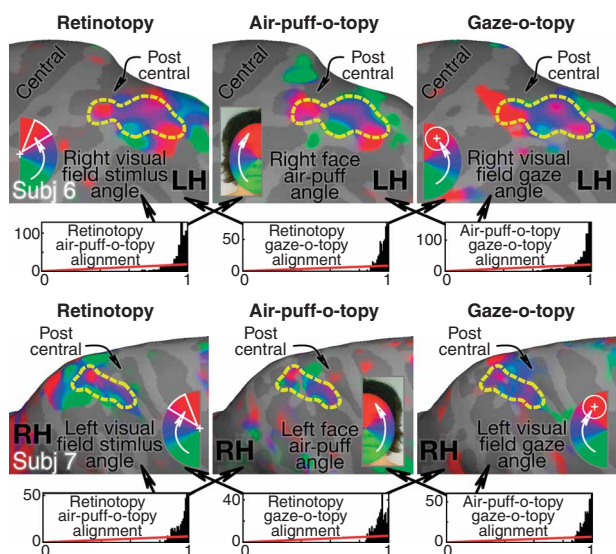


Figure 6 Evidence for head-centered representation in human VIP. Retinotopic maps (left, central fixation with rotating wedge), air-puff maps (middle, eyes closed) and gaze-angle maps (right, constant retinotopic stimulus as subject slowly tracks a moving fixation point) coincide in many details in data from two single subjects (top, bottom). Alignment histograms for each pairwise comparison are shown below each row. The similarity between the ‘gaze-o-topic’ maps and the other two maps suggests that some neurons in VIP may code the location of near-face objects in head-centered coordinates. The thick dashed yellow outlines have been drawn in identical positions.

frontal areas²⁵ in humans. A region near or overlapping our proposed VIP has been activated in a large number of neuroimaging studies and has been given a number of different names (see below). The registered sensory maps demonstrated here may help to more clearly define areal borders in this complex region.

Higher visual areas are often as strongly modulated by visual attention as by actual visual stimuli. For example, the retinotopic activation in area LIP when a subject remembers a target at a location can be as large as the activation there when the subject actually views the target but ignores it¹⁰. Although the visual responses of VIP neurons are modulated by attention²⁶, it seems unlikely that visual attention could explain the activation to facial air puffs seen here in putative human area VIP, as the areas that are most strongly modulated by visual attention—such as LIP+, V7 and V3A—were silent during air-puff stimulation, as was virtually the entire occipital area at the anterior and superior edge of the MT complex, however, was also activated by the air puffs²⁷. It is interesting to note that in macaque monkeys, a motion-sensitive area in this position, MSTd, has been found to have strong connections with VIP (ref. 4).

The aligned somatosensory and visual maps in the human parietal face area provide a straightforward framework for coordinating information about nearby objects in the world. A venerable example of this computational motif is the layering of different sensory modalities in the superior colliculus²⁸. In that case, the goal is to combine multisensory information in a retinocentric coordinate system in order to direct the center of gaze to visual targets worth looking at. Perhaps VIP can be thought of in a similar way, except that multisensory signals there are combined in a head-centered coordinate system for the purpose of approaching, manipulating and avoiding objects with the face^{6–8,29}. It is likely to be a neocortical area of some antiquity given the centrality of saving your face.

METHODS

Subjects. Subjects ($n = 12$) were male and female students, faculty and staff of the University of California, San Diego (UCSD), with normal or corrected-to-normal vision. Each participated in 1–5 fMRI imaging sessions. Informed consent was obtained according to procedures approved by the UCSD Human Research Protections Program.

Somatosensory stimuli and tasks. For somatosensory stimuli, an air compressor in the scanner control room provided input to a 12-way solenoid manifold valve (Numatics) that was controlled by TTL pulses from a stimulus computer parallel port. Twelve plastic air tubes from the manifold valve passed through waveguides into the scanner room and then into the magnet, where they connected to a block mounted on the head coil that served as a rigid base for 12 flexible tubes with nozzles (Loc-Line) that could be freely positioned in order to direct air puffs at 12 locations around the person’s face³⁰. The input air pressure (30–40 psi) was adjusted so that a 500-ms air puff could be reliably detected by the person. The air puffs were perceived as light, slightly cool touches on a localized region of the face. They were presented either in block designs (ON versus OFF, left face versus right face) or in mapping experiments (one cycle around the face, clockwise or counterclockwise, every 64 s) while subjects monitored for occasional gaps in an otherwise equally spaced sequence.

Head-centered representations

Single-unit experiments have shown that the visual receptive fields of some VIP neurons are remapped into head-centered somatosensory coordinates (note that the reverse—remapping somatosensory receptive fields into retinal coordinates—does not occur in VIP). In the experiments described above, subjects maintained central fixation during visual mapping so that no remapping of visual inputs was required to maintain alignment with a head-centered face map. To test whether human VIP shows evidence for head-centered visual receptive field remapping, we had subjects ($n = 6$) track a fixation point in the center of a circular aperture, approximately 20° across, as the aperture moved periodically around the person’s face (Fig. 6, right) along a circular path 50° in diameter. A video was displayed in the aperture. Central retinal stimulation was approximately constant in this case, but the position of the stimulus varied periodically with respect to the head and face. Periodic activation by this stimulus was consistent with a head-centered visual representation. We used the phase of the periodic response to estimate the angle to which the central receptive fields had been remapped, and compared these ‘gaze-o-topic’ maps to retinotopic maps (Fig. 6, left) and air-puff maps (Fig. 6, middle). Inspection of these maps (from the same subject) showed that all three were consistent within each subject. The quantitative alignment index histograms (three-way) and map correlations (Table 1) confirmed this impression. This result was obtained despite the fact that remapping of visual receptive fields is not found in all VIP neurons⁹. We did our best to minimize stray light. However, because a video projector cannot generate a pure (zero brightness) black, the dimly lit masked portion of the projected image may have stimulated the moving retina; however, the phase of such a response would be reversed and offset by 180° and could only have canceled the signal we observed.

DISCUSSION

The multisensory representation of the angular position of both a visual stimulus and a somatosensory stimulus is consistent with data collected in single neurons in macaque area VIP. These data go beyond the nonhuman primate data, however, in suggesting that adjacent locations on the face along with the corresponding adjacent locations in the visual field are mapped to adjacent locations on the cortex in a manner similar to what has been found in early visual areas such as V1 and V2 but also in higher-level parietal areas such as LIP and several

Visual stimuli and tasks. For visual optical flow stimuli, an in-house program (original by A. Dale, UCSD) contrasted 16-s blocks of coherent motion with scrambled motion. A new field of white dots was generated every 500 ms. Dots immediately began to move along a trajectory so as to generate a coherent movement on a plane. The motion was chosen randomly for that 500-ms period from a continuum that ranged from dilations to outward spirals, to rotations, to inward spirals, to contractions. The center of the movement was jittered, and the speed varied within a small range. During the scrambled OFF period, dots and their movement vectors were generated as during the coherent ON periods except that each dot was rotated at a random angle around the pattern center before its path was executed. This scrambled the coherency of movement (at a given point, dots moved in different directions) but preserved the speed gradient (central dots still moved slower than peripheral dots).

For retinotopic visual mapping stimuli, in-house OpenGL programs generated either a standard flashing checkerboard rotating wedge (original by A. Dale) or video wedge stimuli (by M.I.S.) on an SGI O2. In both cases, the wedge moved smoothly. For video, a black mask containing a wedge-shaped aperture 45° wide was drawn on top of each NTSC input frame (from episodes of “Xena the Warrior Princess”) in real time. The aperture slowly rotated around a central fixation cross (one cycle every 64 s). Each video frame was scaled down to the approximate size of the aperture and then translated so that the center of each frame always appeared at the center of the slowly rotating aperture. Subjects fixated a central cross for the duration of the scan (stability verified by tests with a pupillometer outside the scanner) and, in the case of video stimuli, attempted to follow the story.

To test for head-centered visual representations, we had subjects track a fixation point in the center of a circular aperture ~20° wide that contained video (same source as above), while the aperture and superimposed fixation cross moved periodically around the person’s face along a circular path ~50° in diameter. As for the video retinotopy stimulus, video frames were scaled and centered within the aperture before the mask was drawn. Central and near-peripheral retinal stimulation was approximately constant in this case but the stimulus periodically varied its position with respect to the head and face. Periodic activation by this stimulus was consistent with a head-centered visual representation. The phase of the periodic response can be used to estimate the angle to which central receptive fields have been remapped.

Data acquisition and analysis. Echoplanar images were collected during 512-s runs (3-Tesla GE Signa Excite, eight-element phased-array head coil, single shot EPI, 3 × 3 mm² in-plane, 3- to 4-mm-thick slices, 256 images per slice, 31 axial slices, flip angle = 90°, TE = 30 ms, TR = 2,000 ms, 64 × 64 matrix, bandwidth = 1,800 Hz per pixel). A total of 241 functional scans were performed on 12 persons; for each person, these included at least 6 face air-puff scans and 8 scans to map visual areas. Functional scans were motion-corrected using the AFNI program 3dvolreg. FreeSurfer was used to reconstruct the cortical surface for each person from a pair of registered structural scans (FSPGR, 1 × 1 × 1 mm³) taken in a separate session. The last scan of each functional session was an alignment scan (also FSPGR, 1 × 1 × 1.3 mm³) acquired in the plane of the functional scans, and was used to establish an initial registration of the functional data with the surface, which was then refined using manual blink comparison with the structural images to achieve an exact overlay of the functional data onto each cortical surface. To increase the signal-to-noise ratio, we typically combined four 512-s scans for each task.

To determine which areas were significantly activated as well as the phase of that activation, a Fourier transform was computed for the time series at each voxel after removing the linear trend. An *F*-ratio was constructed by comparing the power of the (complex) signal at the stimulus frequency (8 or 16 cycles per scan) to the power of the noise (other frequencies). Very low frequencies (movement artifact) and harmonics³¹ were excluded. The *F*-ratio was then converted to a *P*-value (uncorrected) by considering degrees of freedom of the signal and noise. In two-condition experiments, the phase angle at the stimulus frequency was divided into two bins corresponding to responses to ON and OFF blocks, and the ON phases were displayed using a heat scale ending in white (OFF block responses were negligible in all four two-condition experiments). In mapping experiments, the phase angle was displayed using a continuous color scale (red to blue to green). In both cases, the saturation of the colors was modulated by the *P*-value, as illustrated in the color bar insets in the figures.

Surface-based cross-subject average map. Two nine-person, 32-scan cross-subject average maps were constructed by morphing individual brain surfaces into alignment with an average target brain, sampling the data onto a subtessellated icosahedron, combining the complex signals by vector averaging²⁵ after reversing phase as appropriate (the vector sum strongly penalizes inconsistent phase across scans and corrects for stationary between-voxel differences in hemodynamic delay), and then sampling the statistic back onto an individual brain, all using FreeSurfer. Three of 12 subjects, whose data were most contaminated by movement artifact, were omitted from the average.

The software used in this process is available for free download (binaries for IRIX and Linux) at <http://surfer.nmr.mgh.harvard.edu/>. A download that also includes retinotopy analysis tools is available at <http://kamares.ucsd.edu/~sereno/csurf/tarballs/>. AFNI tools can be found at <http://afni.nimh.nih.gov/afni/>.

To obtain three-dimensional coordinates compatible with previous studies, we used the Montreal Neurological Institute Automated Linear Registration Package to generate Talairach transformation matrices³² available for free download as MNI autoreg at <http://www.bic.mni.mcgill.ca/software/distribution/>. The average Talairach coordinates for the center of mass of VIP across the nine subjects in the right and left hemispheres were (30, 43, 59) and (–28, –46, 58) with standard deviations (4, 5, 6) and (4, 7, 6) (all in mm). Note that different Talairach methods—for example, local feature (AC-PC) versus global correlation (MNI)—give slightly different results because they ‘pay attention’ to different things.

Map alignment measures. To quantitatively compare the alignment between pairs of ‘air-puff-o-topic’, retinotopic and ‘gaze-o-topic’ maps, we calculated alignment indices and correlation coefficients. Both measures were evaluated across a region of interest defined as a connected two-dimensional patch of surface vertices in anterior superior parietal cortex that had a significant periodic response to both phase-encoded air puffs and phase-encoded masked video stimuli. Note that this conservative method of choosing the region of interest is likely to underestimate the overall size of human VIP, as we did not stimulate the entire surface of the face, head and upper body. The alignment index for each pair of vertices was defined as

$$\text{Alignment_index} = 1 - \frac{|\Delta\phi|}{\pi},$$

where $\Delta\phi$ is the difference between the polar angle in the two data sets in radians. This index ranges from 1 (when the polar angle at a vertex is identical in the two data sets) to 0 (when one polar angle is on the upper vertical meridian and the other is on the lower vertical meridian). A histogram of alignment indices for a region of interest that is sharply peaked near 1 indicates that the two maps are well aligned (perfect alignment would be a spike exactly at 1). For two data sets with uncorrelated polar angle maps, by contrast, the distribution of alignment indices is a shallow linear ramp starting at a count of 0 at an alignment index of 0 and ending at a small value ($2v/n$, where v is the number of vertices and n is the number of bins) at an alignment index of 1 (this is illustrated as a red line in each alignment index histogram). The average of the alignment indices (average angular offset) and the standard deviation of angular offsets were calculated for each comparison to roughly characterize the distributions (Table 1). We also calculated a correlation coefficient for vertex-by-vertex polar angles for each comparison (after controlling for angle wraparound), which was strong and highly significant in every instance ($P < 10^{-10}$) (Table 1). We did not attempt to correct for systematic offsets (for example, those due to misalignment of the visual and somatosensory stimuli).

Nomenclature. The nomenclature of areas in human intraparietal sulcus is not completely settled³¹. Here are some correspondences with studies not otherwise mentioned. The most anterior parietal focus in Figure 1 in ref. 33 is very close to VIP as defined here. The area labeled “DIPSA” in Figure 1 of ref. 34 is close to our VIP (the region they label “VIPS” has been labeled V7 in several other studies). The region labeled “VIP/SPO” in Figure 2 of ref. 35 is similar to area V6 as defined in ref. 18 and is posterior and medial to our current VIP. The area labeled “aIPS (VIP/LIP)” in ref. 36 is similar to our VIP.

There appears to be a multisensory cortical area in a similar relative location to VIP in both cats (rostral lateral suprasylvian sulcus, r-LS) and rodents

(rostrolateral, RL). As with VIP, these areas lie at the border between unimodal visual and somatosensory areas, they are anterior and superior to most other extrastriate visual areas, and they are distinctly medial to the representation of the face in primary somatosensory cortex. In cats, area r-LS, which is just posterior to the fifth somatosensory area (SV, not equivalent to area 5), receives input from motion-sensitive lateral suprasylvian areas just posterior to it as well as registered somatosensory inputs^{37,38}. In rats, area RL contains a mostly lower visual field representation superimposed on a representation of the vibrissae (ref. 39; and M.I.S. and J. Olavarria Univ. of Washington, Seattle, unpublished data).

Cortical connections with area VIP in monkeys⁴ include (i) areas sensitive to visual motion (PO/V6, MDP, MSTd, FST and LIP), (ii) areas that could be the source of somatosensory input from the face (strong connections from 5 and 7b, and moderate from S-II and area 2), and (iii) anterior areas associated with movements of the face and eyes (areas 4 and 6, cingulate motor area 24d). Frontal connections include the recently described polysensory area on the precentral gyrus⁵ that has been shown to modulate defensive movements of the face and torso.

Note: Supplementary information is available on the Nature Neuroscience website.

ACKNOWLEDGMENTS

We thank D. Hagler for developing the concept and software implementation of cross-subject averaging of complex-valued data on morphed surfaces; R. Buxton, E. Wong, T. Liu and L. Frank at the University of California San Diego fMRI Center for scan time, pulse sequences and advice; L. May and R. Kurz for technical assistance; A. Dale, S. Pitzalis, F. Dick and A. Chiba for help and discussions; and L. Kemmer for pilot experiments. Supported by National Science Foundation BCS 0224321 (M.I.S.); US National Institutes of Health R01 NS41925 (E.W.), R01 NS36722 (R.B.) and R01 HD041581 (J.S.); and the Swartz Foundation (T.-P.J.).

AUTHOR CONTRIBUTIONS

The authors contributed equally to this work.

COMPETING INTERESTS STATEMENT

The authors declare that they have no competing financial interests.

Published online at <http://www.nature.com/natureneuroscience>

Reprints and permissions information is available online at <http://npg.nature.com/reprintsandpermissions/>

1. Duhamel, J.R., Colby, C.L. & Goldberg, M.E. Ventral intraparietal area of the macaque: congruent visual and somatic response properties. *J. Neurophys.* **79**, 126–136 (1998).
2. Colby, C.L., Duhamel, J.R. & Goldberg, M.E. Ventral intraparietal area of the macaque: anatomic location and visual response properties. *J. Neurophys.* **69**, 902–914 (1993).
3. Bremmer, F., Duhamel, J.R., Ben Hamed, S. & Graf, W. Heading encoding in the macaque ventral intraparietal area (VIP). *Eur. J. Neurosci.* **16**, 1554–1568 (2002).
4. Lewis, J.W. & Van Essen, D. Corticocortical connections of visual, sensorimotor, and multimodal processing areas in the parietal lobe of the macaque monkey. *J. Comp. Neurol.* **428**, 112–137 (2000).
5. Cooke, D.F. & Graziano, M.S. Super-flinchers and nerves of steel: defensive movements altered by chemical manipulation of a cortical motor area. *Neuron* **43**, 585–593 (2004).
6. Cooke, D.F., Taylor, C.S., Moore, T. & Graziano, M.S. Complex movements evoked by microstimulation of the ventral intraparietal area. *Proc. Natl. Acad. Sci. USA* **100**, 6163–6168 (2003).
7. Bremmer, F. Navigation in space—the role of the macaque ventral intraparietal area. *J. Physiol. (Lond.)* **566**, 29–35 (2005).
8. Grefkes, C. & Fink, G.R. The functional organization of the intraparietal sulcus in humans and monkeys. *J. Anat.* **207**, 3–17 (2005).
9. Avillac, M., Deneve, S., Olivier, E., Pouget, A. & Duhamel, J.R. Reference frames for representing visual and tactile locations in parietal cortex. *Nat. Neurosci.* **8**, 941–949 (2005).
10. Colby, C.L., Duhamel, J.R. & Goldberg, M.E. Visual, presaccadic, and cognitive activation of single neurons in monkey lateral intraparietal area. *J. Neurophysiol.* **76**, 2841–2852 (1996).
11. Grunewald, A., Linden, J.F. & Andersen, R.A. Responses to auditory stimuli in macaque lateral intraparietal area. I. Effects of training. *J. Neurophysiol.* **82**, 330–342 (1999).
12. Bremmer, F. *et al.* Polymodal motion processing in posterior parietal and premotor cortex: a human fMRI study strongly implies equivalencies between humans and monkeys. *Neuron* **29**, 287–296 (2001).
13. Culham, J.C. & Kanwisher, N.G. Neuroimaging of cognitive functions in human parietal cortex. *Curr. Opin. Neurobiol.* **11**, 157–163 (2001).
14. Sereno, M.I., Pitzalis, S. & Martinez, A.M. Mapping of contralateral space in retinotopic coordinates by a parietal cortical area in humans. *Science* **294**, 1350–1354 (2001).
15. Merriam, E.P., Genovesi, C.R. & Colby, C.L. Spatial updating in human parietal cortex. *Neuron* **39**, 361–373 (2003).
16. Medendorp, W.P., Goltz, H.C., Vilis, T. & Crawford, J.D. Gaze-centered updating of visual space in human parietal cortex. *J. Neurosci.* **23**, 6209–6214 (2003).
17. Sereno, M.I. *et al.* Borders of multiple visual areas in humans revealed by functional magnetic resonance imaging. *Science* **268**, 889–893 (1995).
18. Pitzalis, S. *et al.* Wide-field retinotopy defines human cortical visual area V6. *J. Neurosci.* **26**, 7962–7973 (2006).
19. Schluppeck, D., Glimcher, P. & Heeger, D.J. Topographic organization for delayed saccades in human posterior parietal cortex. *J. Neurophysiol.* **94**, 1372–1384 (2005).
20. Hasson, U., Nir, Y., Levy, I., Fuhrmann, G. & Malach, R. Intersubject synchronization of cortical activity during natural vision. *Science* **303**, 1634–1640 (2004).
21. Engel, S.A. *et al.* fMRI of human visual cortex. *Nature* **369**, 525 (1994).
22. Fischl, B., Sereno, M.I., Tootell, R.B. & Dale, A.M. High-resolution intersubject averaging and a coordinate system for the cortical surface. *Hum. Brain Mapp.* **8**, 272–284 (1999).
23. Hagler, D.J., Riecke, L. & Sereno, M.I. Pointing and saccades rely on common parietal and superior frontal visuospatial maps. *Neuroimage* (in the press).
24. Gattass, R. *et al.* Cortical visual areas in monkeys: location, topography, connections, columns, plasticity and cortical dynamics. *Philos. Trans. R. Soc. Lond. B Biol. Sci.* **360**, 709–731 (2005).
25. Hagler, D.J. & Sereno, M.I. Spatial maps in frontal and prefrontal cortex. *Neuroimage* **29**, 567–577 (2006).
26. Cook, E.P. & Maunsell, J.H. Attentional modulation of behavioral performance and neuronal responses in middle temporal and ventral intraparietal areas of macaque monkey. *J. Neurosci.* **22**, 1994–2004 (2002).
27. Beauchamp, M. See me, hear me, touch me: multisensory integration in lateral occipital-temporal cortex. *Curr. Opin. Neurobiol.* **15**, 145–153 (2005).
28. Calvert, G.A., Spence, C. & Stein, B.E. (eds.) *Handbook of Multisensory Processing* (MIT Press, Cambridge, Massachusetts, 2004).
29. Spence, C. & Driver, J. (eds.) *Crossmodal Space and Crossmodal Attention* (Oxford Univ. Press, Oxford, 2004).
30. Huang, R.-S. & Sereno, M.I. Dodecapus: an MR-compatible system for somatosensory stimulation. *Neuroimage* (in the press).
31. Sereno, M.I. & Tootell, R.B. From monkeys to humans: what do we now know about brain homologies? *Curr. Opin. Neurobiol.* **15**, 135–144 (2005).
32. Collins, D.L., Neelin, P., Peters, T.M. & Evans, A.C. Automatic 3D intersubject registration of MR volumetric data in standardized Talairach space. *J. Comput. Assist. Tomogr.* **18**, 192–205 (1994).
33. Culham, J.C. *et al.* Cortical fMRI activation produced by attentive tracking of moving targets. *J. Neurophysiol.* **80**, 2657–2670 (1998).
34. Orban, G.A. *et al.* Similarities and differences in motion processing between the human and macaque brain: evidence from fMRI. *Neuropsychologia* **41**, 1757–1768 (2003).
35. Tootell, R.B., Dale, A.M., Sereno, M.I. & Malach, R. New images from human visual cortex. *Trends Neurosci.* **19**, 481–489 (1996).
36. Astafiev, S.V. *et al.* Functional organization of human intraparietal and frontal cortex for attending, looking, and pointing. *J. Neurosci.* **23**, 4689–4699 (2003).
37. Mori, A. *et al.* Fifth somatosensory cortex (SV) representation of the whole body surface in the medial bank of the anterior suprasylvian sulcus of the cat. *Neurosci. Res.* **11**, 198–208 (1991).
38. Monteiro, G.A., Clemo, H.R. & Meredith, M.A. Anterior ectosylvian cortical projections to the rostral suprasylvian multisensory zone in cat. *Neuroreport* **14**, 2139–2145 (2003).
39. Thomas, H.C. & Espinoza, S.G. Relationships between interhemispheric cortical connections and visual areas in hooded rats. *Brain Res.* **417**, 214–224 (1987).

